TWO-TIME-LEVEL SEMI-LAGRANGIAN SCHEMES FOR FINITE-ELEMENT AND SPECTRAL MODELS

Andrew Staniforth and Jean Côté
Division de Recherche en Prévision Numérique
Service de l'Environnement Atmosphérique
Dorval, Québec, Canada H9P 1J3

1. INTRODUCTION

The need for higher-resolution numerical weather forecasts motivated Robert (1981, 1982) to propose the coupling of a semi-Lagrangian treatment of advection (where stability is no longer limited by the magnitude of the horizontal wind) with a semi-implicit treatment of gravitational oscillations. This idea was first demonstrated in the context of a shallow-water equations gridpoint model, and later extended to the baroclinic primitive equations (Bates and McDonald, 1982; Robert et al., 1985).

During the last several years a number of investigators have pursued the stability advantages of semi-Lagrangian advection in different contexts. Further applications of the technique to gridpoint models may be found in Bates (1984), McDonald (1986), Ritchie (1986) and Bates (1988). Recently the method has been extended to include both finite-element (Staniforth and Temperton, 1986) and spectral (Ritchie 1987, 1988) methodologies. Semi-Lagrangian advection has also been proposed for pollutant transport problems (Pudykiewicz et al., 1985) and moisture advection (Ritchie, 1985).

Present semi-Lagrangian schemes are based on discretization over either two or three time levels. Two-time-level schemes are potentially twice as efficient and simpler to code than three-time-level schemes and

additionally have no time computational modes. In practice however the advantages of two-time-level schemes over three-time-level ones were not fully realized by the early two-time-level schemes, due to the difficulty in obtaining 2nd-order accurate ($O(\Delta t^2)$) trajectories (Staniforth and Pudykiewicz, 1985; McDonald, 1987). Independently Temperton and Staniforth (1987) and McDonald and Bates (1987) proposed a 2nd-order accurate method of obtaining the trajectories for two-time-level models, and this approach has been pursued by Purser and Leslie (1988) for gridpoint regional models. Such an approach offers a potential doubling of efficiency with respect to three-time-level schemes. This was demonstrated by Temperton and Staniforth (1987) for a shallow-water finite-element-model, and by Côté and Staniforth (1988) for a spectral shallow-water model. In these two-time-level schemes, all the linear terms are treated implicitly, while the non-linear terms are either treated explicitly using time-extrapolated values or implicitly via iteration. The resulting algorithm is unconditionally stable (in the linear sense) which allows the timestep to be chosen on the basis of accuracy alone. The purpose of the present paper is to present the basic ideas of this approach, together with some substantiating results, and to compare them with those of the companion paper of Temperton and Ritchie (1988) for three-time-level schemes.

2. APPLICATION TO A SHALLOW WATER FINITE-ELEMENT MODEL

2.a Governing equations

We first examine the application of a two-time-level semi-implicit/semi-Lagrangian scheme to a finite-element model of the shallow-water equations on a polar-stereographic projection. The governing equations and notation are as in the companion paper of Temperton and Ritchie (1988). Thus

$$\frac{dU}{dt} + \phi_x - fV = -KS_x, \tag{2.1}$$

$$\frac{dV}{dt} + \phi_y + fU = -KS_y, \tag{2.2}$$

$$\frac{d}{dt}(\ln\phi) + D = 0, \tag{2.3}$$

where

$$K = \tfrac{1}{2}(U^2+V^2),\ S = m^2,\ D = S(U_x+V_y) \text{ and}$$

$$\frac{d}{dt} = \frac{\partial}{\partial t} + S\left(U\frac{\partial}{\partial x}+V\frac{\partial}{\partial y}\right).$$

Suppose that the model variables U, V, ϕ are defined at a set of grid points at time levels t, $(t-\Delta t)$, $(t-2\Delta t)$,..., and that the integration is to be carried forward to time-level $(t+\Delta t)$. For each gridpoint $\underset{\sim}{x}$, we consider the trajectory of a particle which arrives at $\underset{\sim}{x}$ at time $(t+\Delta t)$, and we approximate this trajectory by a straight line in (x, y) space over the time interval $[t, t+\Delta t]$ as illustrated in Fig. 1. Thus in (x, y, t) space, the trajectory begins at $(\underset{\sim}{x}-\underset{\sim}{\alpha}, t)$ and ends at $(\underset{\sim}{x}, t+\Delta t)$.

2.b Trajectory calculations

To implement the semi-Lagrangian algorithm, the first step is to determine the displacements $\underset{\sim}{\alpha}$ by approximate integration of

$$\frac{d\underset{\sim}{x}}{dt} = \underset{\sim}{V} = (SU, SV). \tag{2.4}$$

Perhaps the simplest such approximation (method 1) is that of Bates and McDonald (1982), where $\underset{\sim}{\alpha}$ is computed explicitly from the relation

$$\underset{\sim}{\alpha} = \Delta t\underset{\sim}{V}(\underset{\sim}{x},t). \tag{2.5}$$

However, as we show later, method 1 leads to serious truncation errors when used with large timesteps.

Since enhanced stability is of little benefit if achieved at the expense of accuracy, we examine various alternatives for improving the accuracy of the trajectory computations. A straightforward method (method 2) is to extrapolate the winds at mesh points to time $(t+\frac{1}{2}\Delta t)$ using

$$\underset{\sim}{V}(\underset{\sim}{x},t+\tfrac{1}{2}\Delta t) = \tfrac{1}{2}[3\underset{\sim}{V}(\underset{\sim}{x},t) - \underset{\sim}{V}(\underset{\sim}{x},t-\Delta t)] \tag{2.6}$$

and then to solve iteratively

$$\underset{\sim}{\alpha} = \Delta t V(\underset{\sim}{x}-\tfrac{1}{2}\underset{\sim}{\alpha},t+\tfrac{1}{2}\Delta t) \tag{2.7}$$

for $\underset{\sim}{\alpha}$, using interpolation to evaluate quantities at $(\underset{\sim}{x}-\frac{1}{2}\underset{\sim}{\alpha})$. Experiments show only small differences between linear and cubic interpolation in our trajectory computations. This iterative procedure is similar to that introduced by Robert (1981), and discussed in the companion paper. A sufficient condition for convergence is given in Pudykiewicz et al. (1985).

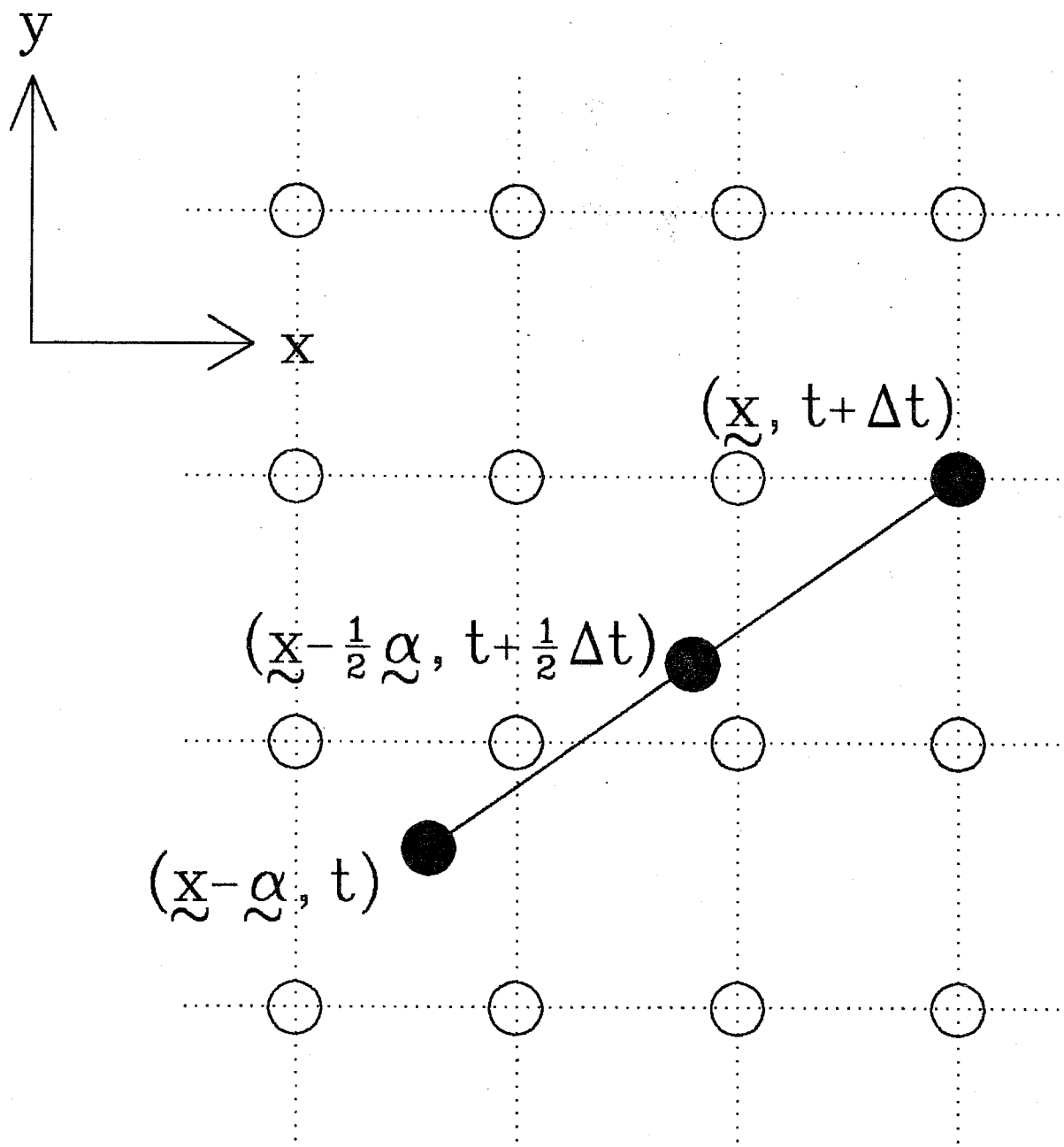

Fig. 1 Two-dimensional trajectory. Departure point - $(\underset{\sim}{x}-\underset{\sim}{\alpha},t)$; arrival point - $(\underset{\sim}{x},t+\Delta t)$.

Extending method 2, we replace the two-time-level extrapolation (2.6) by the three-time-level extrapolation

$$\underset{\sim}{V}(\underset{\sim}{x},t+\tfrac{1}{2}\Delta t) = (1/8)[15\underset{\sim}{V}(\underset{\sim}{x},t)-10\underset{\sim}{V}(\underset{\sim}{x},t-\Delta t)+3\underset{\sim}{V}(\underset{\sim}{x},t-2\Delta t)] \qquad (2.8)$$

in the iterative solution of (2.7). This method (method 3) turns out to yield the most accurate trajectories of the various methods tried. All of these extrapolation schemes yield winds at $(t+\tfrac{1}{2}\Delta t)$, which can also be used to compute the time-centred metric terms in (2.1) and (2.2).

2c. Discretisation of governing equations

Once $\underset{\sim}{\alpha}$ has been found, the total derivatives can be approximated by

$$\frac{dF}{dt} \rightarrow \frac{F^+-F^-}{2\Delta t}, \qquad (2.9)$$

where

$$F^+ = F(\underset{\sim}{x},t+\Delta t), \qquad (2.10)$$

$$F^- = F(\underset{\sim}{x}-\underset{\sim}{\alpha},t). \qquad (2.11)$$

Here F^+ is F evaluated at the arrival point (a meshpoint) and F^- is F evaluated (by cubic interpolation) at the departure point.

The discretisation of (2.1) - (2.3) is analogous to that of the companion paper. It consists of taking time averages and differences for the terms on the left-hand-sides and evaluating the right-hand-sides midway along the trajectories. The principal differences are that these averages and differences are taken over a time interval of Δt rather than $2\Delta t$, that the Coriolis terms are time-averaged rather than explicitly evaluated, and that the metric terms (which are small for this projection) are evaluated using extrapolated values for the winds. Regarding this latter point it is possible to avoid calculating these terms explicitly and this is described in Côté (1988): the discretisation is then a Crank-Nicolson one along the trajectories. Results using the two methods are virtually indistinguishable and are quantified in Côté (1988).

Eqs. (2.1)-(2.3) are thus discretised as

$$\frac{U^+-U^-}{\Delta t} + \tfrac{1}{2}(\phi_x^+ + \phi_x^-) - \tfrac{1}{2}[(fV)^+ + (fV)^-] = -(KS_x)^\circ, \qquad (2.12)$$

$$\frac{V^+-V^-}{\Delta t} + \tfrac{1}{2}(\phi_y^+ + \phi_y^-) + \tfrac{1}{2}[(fU)^+ + (fU)^-] = -(KS_y)^\circ, \qquad (2.13)$$

$$\frac{(\ln\phi)^+-(\ln\phi)^-}{\Delta t} + \tfrac{1}{2}(D^+ + D^-) = 0 \qquad (2.14)$$

where $(\,)^\circ$ denotes evaluation at the midpoint $(\underset{\sim}{x}-\tfrac{1}{2}\underset{\sim}{\alpha}, t+\tfrac{1}{2}\Delta t)$ of the trajectory.

Manipulation of (2.12) - (2.14) leads to a single (elliptic) equation for ϕ^+ (see Temperton and Staniforth, 1987 for details), viz.

$$(a\phi_x^+)_x + (a\phi_y^+)_y + (b\phi_y^+)_x - (b\phi_x^+)_y - \frac{4(\ln\phi)^+}{S(\Delta t)^2} = \text{known}, \qquad (2.15)$$

where $a = 1/[1+(\tfrac{1}{2}f\Delta t)^2]$ and $b = \tfrac{1}{2}f\Delta t a$. This equation is solved for ϕ^+ and the winds are obtained in an analogous way to that of the companion paper. Details again may be found in Temperton and Staniforth (1987).

2.d Analysis of scheme

It can be shown (Temperton and Staniforth, 1987; McDonald, 1987) that the time truncation error of the scheme depends on the method used to calculate the trajectories. Using method 1 leads to only first-order accuracy in time, whereas methods 2 and 3 yield second-order accuracy.

2.e Results

The experimental procedure closely follows that of the companion paper. Thus, the model was run over a square domain of side 20 000km centred at the north pole, using a stereographic projection true at 60°N and bounded by a solid wall in the vicinity of the equator. This domain was covered by a non-uniform mesh of 101x101 points, with a 61x61 uniform high-resolution (100km) mesh over the North American 'area of interest' (see Fig. 2 of the companion paper). The same carefully balanced initial conditions as before were used, based on an operational 500 mb analysis for 12 GMT on 28 February 1984. The model was run to 48 hours with various choices of the scheme for calculating displacements, and with various timestep lengths.

To evaluate the results obtained using variants of the described scheme on the non-uniform grid, the forecasts were compared against those of a control run on a uniform 201x201 100km mesh covering the same domain. This control run used the three-time-level semi-implicit Eulerian formulation of Staniforth and Mitchell (1977, 1978), with a timestep small enough (Δt=10min) to make the time truncation errors negligible.

For a preliminary assessment of the accuracy of the schemes, we present in Fig. 2 a series of maps of the forecast height field after 48 hours. Figure 2(a) shows the 'control' forecast using the Eulerian scheme on a uniform high-resolution grid with a small timestep. The remaining forecasts all used the non-uniform grid. Figure 2(b) shows the forecast using scheme B of the companion paper with a timestep of 90 minutes. Over the North American high-resolution 'window' the forecast appears identical to the control run, with only small differences over the outer low-resolution areas. Since scheme B is a centred three-time-level scheme, time-derivatives are evaluated over an interval of $2\Delta t$=3 hours, and the goal is to obtain similar accuracy using a two-time-level scheme with a 3-hour timestep.

Figure 2(c) shows the forecast using the two-time-level scheme together with method 1 for the displacement calculations, and a timestep of 10 minutes. Even with such a small timestep the errors are considerable (e.g. 4 dam in the central value for the low over Quebec). Experiments with larger timesteps showed a clear $O(\Delta t)$ growth of the errors, and this method is evidently inadequate for our purposes.

Figure 2(d) shows the corresponding forecast with a timestep of three hours, using method 2 (two-time-level extrapolation) for the displacement calculations. This forecast, though reasonable in view of the large timestep, is by no means as accurate as that of scheme B with half the timestep shown in Figure 2(b).

For the forecast shown in Figure 2(e), a timestep of three hours is again used but with method 3 (three-time-level extrapolation) for the displacement calculations. With this scheme the goal was achieved, in that the control forecast was reproduced with essentially the same accuracy as that of scheme B with half the timestep.

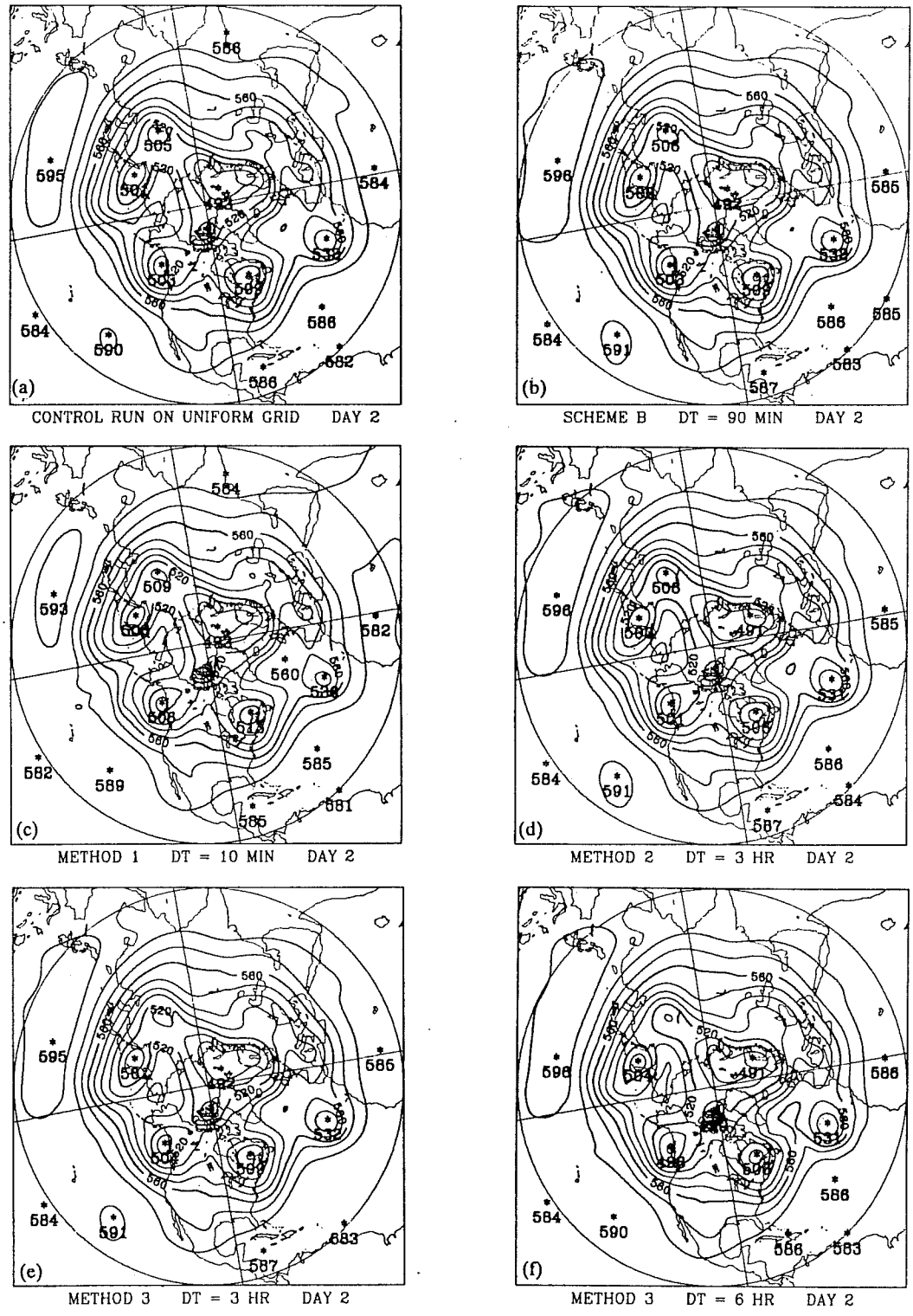

Fig. 2 Forecast geopotential height fields at 48 hours (contour interval 10 dam).

(a) Control run on uniform grid (all other forecasts on non-uniform grid);
(b) Scheme B of companion paper with Δt = 90 mins;
(c) New scheme with method 1 for displacements and Δt = 10 mins;
(d) New scheme with method 2 and Δt = 3 hours;
(e) New scheme with method 3 and Δt = 3 hours;
(f) New scheme with method 3 and Δt = 6 hour.

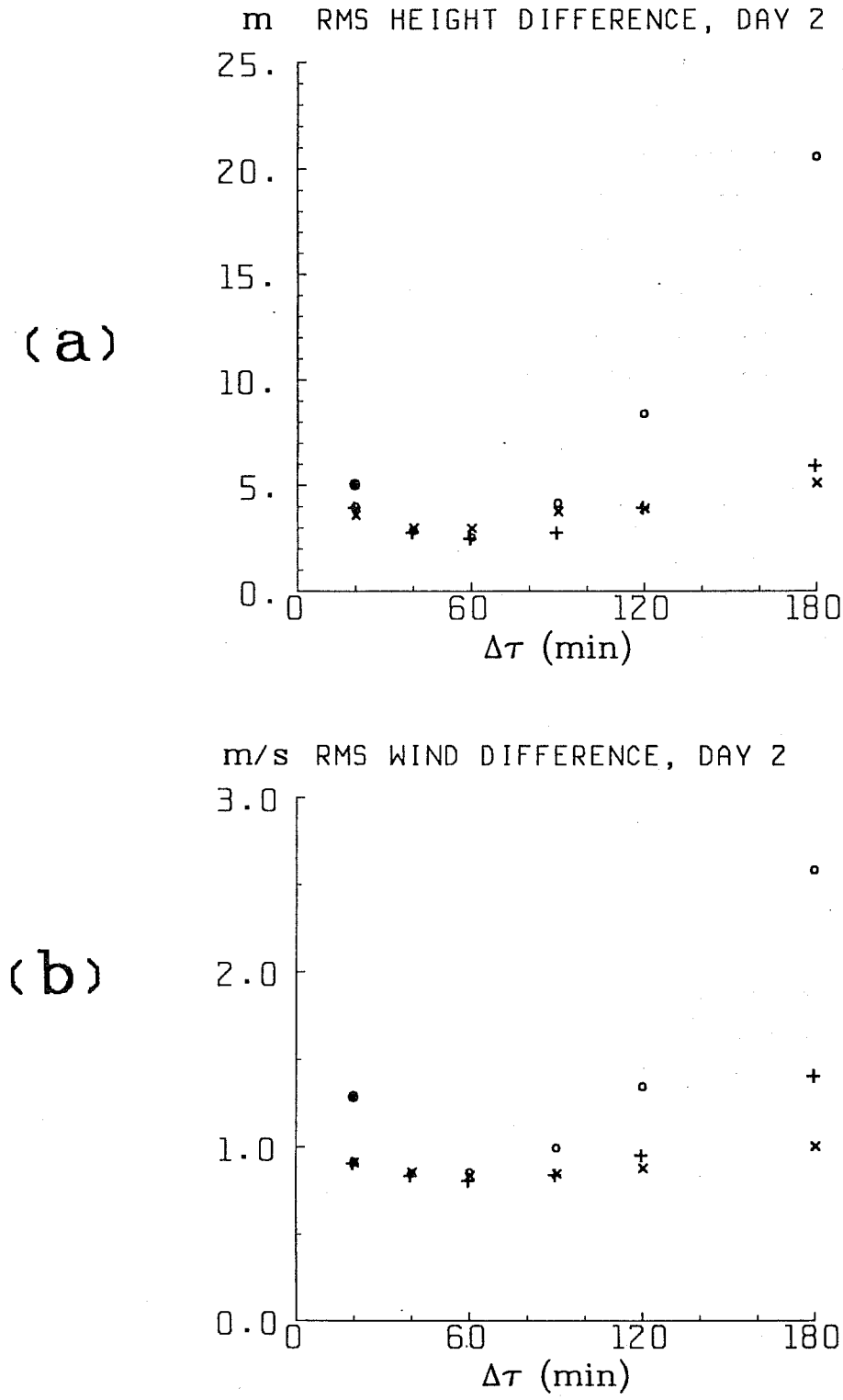

Fig. 3 (a) R.m.s. differences (m) from control run, in the height field over region of interest at 48 hours, as a function of $\Delta\tau$. • Eulerian; x Scheme B; 0 New scheme with method 2 for displacements; + New scheme with method 3.
(b) As (a) but wind field (ms^{-1}).

Finally, Figure 2(f) shows the corresponding forecast using method 3 with a timestep of six hours. The error level is now unacceptable, but we show the figure to make the point that this scheme produces a forecast which is stable and not completely unreasonable, using a timestep 30 times longer than the stability limit for an Eulerian semi-implicit scheme at the same horizontal resolution. With such a scheme we are clearly in a better position to choose the timestep on the basis of balancing the temporal and spatial truncation errors, rather than being constrained by considerations of stability.

In order to investigate the growth of the time-truncation error as a function of timestep length of the two-time-level scheme using methods 2 and 3, a series of forecasts were run on the non-uniform grid with different values of Δt. The accuracy of each forecast was measured by computing the r.m.s. differences (in the height and wind fields) from the control forecast run on the uniform high-resolution grid with a small timestep. The r.m.s. differences were computed over the 'area of interest' where the non-uniform and uniform grids coincide.

The results at 48 hours are plotted in Figs. 3(a) and (b) for the height and wind fields respectively. As a comparison is made with the corresponding results of a three-time-level scheme, we have chosen to plot the r.m.s. differences as a function of $\Delta\tau$, the interval over which time-derivatives are calculated. Thus $\Delta\tau=\Delta t$ for the two-time-level schemes, but $\Delta\tau=2\Delta t$ for a three-time-level scheme. For a given value of $\Delta\tau$, the two-time-level scheme requires approximately half the work of the three-time-level scheme, but the time-truncation errors are in principle formally equivalent.

In Figs. 3(a) and (b), the solid circles plotted at $\Delta\tau$=20min show the r.m.s. difference from the control run for a forecast using the same Eulerian scheme but on the non-uniform grid. Since the timestep is small, this provides an approximate measure of the spatial truncation error incurred by running with lower resolution outside the area of interest.

The crosses show the results for the three-time-level scheme B of the companion paper. As seen in this paper, the forecast over the area of interest using this scheme, with timesteps of at least one hour ($\Delta\tau$=120min), was more accurate than that of the small-timestep Eulerian scheme, and was still of comparable accuracy with a timestep of 90 minutes ($\Delta\tau$=180min).

The goal of the study was to reproduce this level of accuracy with half the computational work, using a two-time-level scheme. The results using method 2 (two-time-level extrapolation) for the displacements are shown in Figs. 3(a) and (b) by open circles. For timesteps ($\Delta\tau$) of up to 90 minutes, the goal is clearly achieved, while for longer timesteps the growth of time-truncation errors becomes evident. Nevertheless, this extrapolation scheme might well be adequate if, for example, a smaller timestep is chosen in a more complete model to resolve the time-evolution of physical processes.

The results using method 3 (three-time-level extrapolation) for the displacements are shown by the 'plus' symbols. This scheme yields acceptable accuracy with timesteps as long as three hours ($\Delta\tau$=180min); the r.m.s. differences are similar to those of scheme B throughout the range, while remaining lower than or similar to those of the corresponding semi-implicit Eulerian scheme with a much smaller timestep. It seems from these results that the optimal timestep at this resolution is approximately three hours, since the spatial and time truncation errors contribute about equally to the total error. There seems to be little virtue in using timestep greater than three hours since the time truncation errors will become dominant.

3. APPLICATION TO A SHALLOW-WATER SPECTRAL MODEL

In the previous section we showed that the two-time-level scheme is twice as efficient as the analogous three-time-level one for comparable accuracy, in the context of a shallow-water finite-element model. In this section we describe how to achieve the same doubling of efficiency in the context of a shallow-water spectral model.

3.a Governing equations

The governing equations are the shallow-water equations on a rotating sphere of radius a. We write the momentum equation in 3-D vector form using the undetermined Lagrange multiplier method as in Côté (1988) and the continuity equation in logarithmic form as in the previous section. Thus in standard notation

$$\frac{d}{dt}\underset{\sim}{V} = \underset{\sim}{F} + \mu\,\underset{\sim}{r}, \tag{3.1}$$

$$\frac{d}{dt}\ln\phi + \underset{\sim}{\nabla}\cdot\underset{\sim}{V} = 0. \tag{3.2}$$

In the above $\underset{\sim}{r}$ is the normalized position vector whose components in a Cartesian frame of reference fixed at the center of the sphere are,

$$\begin{aligned} x &= \cos\lambda\,\cos\theta, \\ y &= \sin\lambda\,\cos\theta, \\ z &= \sin\theta, \end{aligned} \tag{3.3}$$

where λ is the longitude and θ the latitude,

$$\underset{\sim}{V} = a\,\frac{d}{dt}\,\underset{\sim}{r}, \tag{3.4}$$

$$\underset{\sim}{F} = -2\Omega\sin\theta\;\underset{\sim}{r}\times\underset{\sim}{V} - \underset{\sim}{\nabla}\phi, \tag{3.5}$$

and μ is a Lagrange multiplier determined by requiring that the fluid elements remain on the sphere, i.e.

$$\underset{\sim}{r}\cdot\underset{\sim}{r} = 1, \tag{3.6}$$

for all time. The Lagrange multiplier could be determined at this stage but as noted in Côté (1988) it is preferable to determine it after discretisation.

The constraint (3.6) implies that $\underset{\sim}{V}$ is tangent to the sphere at $\underset{\sim}{r}$, and therefore

$$\underset{\sim}{r}\cdot\underset{\sim}{v} = 0. \tag{3.7}$$

This means that the 3-D wind vector has only two independent components which we write in terms of the wind images U and V. Thus

$$\underset{\sim}{V} = \frac{1}{\cos\theta}\,(U\hat{e}_\lambda + V\hat{e}_\theta) \tag{3.8}$$

where $\hat{e}_\lambda$ and $\hat{e}_\theta$ are eastward and northward pointing unit vectors respectively. Introducing the Helmholtz decomposition of $\underset{\sim}{V}$ in terms of the streamfunction ψ and the velocity potential χ, we have

$$\underset{\sim}{V} = \underset{\sim}{r} \times \underset{\sim}{\nabla}\psi + \underset{\sim}{\nabla}\chi, \tag{3.9}$$

$$U = \frac{1}{a}\left(\frac{\partial\chi}{\partial\lambda} - \cos\theta\,\frac{\partial\psi}{\partial\theta}\right), \tag{3.10a}$$

$$V = \frac{1}{a}\left(\frac{\partial\psi}{\partial\lambda} + \cos\theta\,\frac{\partial\chi}{\partial\theta}\right), \tag{3.10b}$$

$$\zeta = \underset{\sim}{r}\cdot(\underset{\sim}{\nabla}\times\underset{\sim}{V}) = \nabla^2\psi, \tag{3.11a}$$

and

$$D = \underset{\sim}{\nabla}\cdot\underset{\sim}{V} = \nabla^2\chi. \tag{3.11b}$$

3.b Semi-Lagrangian discretisation

If we know the trajectory of the fluid element that is at position $\underset{\sim}{r}^+$ at forecast time $(t+\Delta t)$, then Eqs. (3.1) and (3.2) may be integrated following the motion over a time interval Δt. Thus

$$\underset{\sim}{V}^+ - \tfrac{1}{2}\Delta t\,\underset{\sim}{F}^+ = \underset{\sim}{V}^- + \tfrac{1}{2}\Delta t\,\underset{\sim}{F}^- + \tfrac{1}{2}\mu\Delta t(\underset{\sim}{r}^+ + \underset{\sim}{r}^-) = \underset{\sim}{R}, \tag{3.12}$$

$$(\ln\phi)^+ + \tfrac{1}{2}\Delta t D^+ = (\ln\phi)^- - \tfrac{1}{2}\Delta t D^-, \tag{3.13}$$

where $\underset{\sim}{r}^-$ is the upstream position at time t of the fluid element arriving at $\underset{\sim}{r}^+$ at time $(t+\Delta t)$ and the negative superscript denotes evaluation at position $\underset{\sim}{r}^-$ and time t. The Lagrange multiplier is determined by projecting the discretised equation (3.12) onto $\underset{\sim}{r}^+$. Since for constrained motion $\underset{\sim}{V}^+$ and $\underset{\sim}{F}^+$ are both orthogonal to $\underset{\sim}{r}^+$, then so is $\underset{\sim}{R}$ and

$$\mu = -\frac{2}{\Delta t}\,\frac{\underset{\sim}{r}^+\cdot\left(\underset{\sim}{V}^- + \frac{\Delta t}{2}\,F^-\right)}{\left(1 + \underset{\sim}{r}^+\cdot\underset{\sim}{r}^-\right)}\,. \tag{3.14}$$

3.c Trajectory calculations

To complete the discretisation we need to find the trajectory. A sufficiently accurate estimate of the trajectory is obtained by integrating (3.1) and (3.4) subject to (3.6) over the interval $[t,\ t+\Delta t]$ while

neglecting $\underset{\sim}{F}$. The solutions are great circles whose parameters are determined by the wind field at $(t+\frac{1}{2}\Delta t)$ for a centred scheme. The midpoint $\underset{\sim}{r}^{o}$ of the trajectory is obtained by iteratively solving

$$\underset{\sim}{r}^{o} = \cos\Theta\ \underset{\sim}{r}^{+} + \sin\Theta\ \underset{\sim}{r}^{+} \times \frac{(\underset{\sim}{r}^{+}\times\underset{\sim}{V}^{o})}{\left|\underset{\sim}{r}^{+}\times\underset{\sim}{V}^{o}\right|}\ , \tag{3.15}$$

where

$$\underset{\sim}{V}^{o} = \underset{\sim}{V}(\underset{\sim}{r}^{o},\ t+\tfrac{1}{2}\Delta t)\ , \tag{3.16}$$

$$\Theta\ = \tfrac{1}{2}\frac{\left|\underset{\sim}{V}^{o}\right|}{a}\Delta t\ . \tag{3.17}$$

Geometrically we search for a point $\underset{\sim}{r}^{o}$ situated a distance $\frac{1}{2}\left|\underset{\sim}{V}^{o}\right|\Delta t$ upstream on the sphere such that $\underset{\sim}{r}^{+}$, $\underset{\sim}{r}^{o}$ and $\underset{\sim}{V}^{o}$ are coplanar. The point $\underset{\sim}{r}^{-}$ is then

$$\underset{\sim}{r}^{-} = 2\ (\underset{\sim}{r}^{+}\cdot\underset{\sim}{r}^{o})\underset{\sim}{r}^{o} - \underset{\sim}{r}^{+}. \tag{3.18}$$

Eq. (3.15) differs from what was done in Ritchie (1988) where the trajectories are first approximated by straight lines on a tangent plane followed by a correction to come back to the sphere; the computational cost of the two algorithms is almost identical. The impact of algorithmic choice is also negligible, giving rise to r.m.s. height differences of only 20 cm for a 5-day integration of a global T126 spectral model with a 2 h timestep.

As in the previous section we use time extrapolated values for $\underset{\sim}{V}^{o}$. This is the key step of the algorithm that allows a saving of a factor of 2 over the usual semi-implicit semi- Lagrangian algorithm where we need to forecast the wind at time $(t+\frac{1}{2}\Delta t)$. We examine constant (one-term), linear (two-term) and quadratic (three-term) extrapolation, viz

$$\underset{\sim}{V}(\underset{\sim}{r},t+\tfrac{1}{2}\Delta t) = c_1\underset{\sim}{V}(\underset{\sim}{r},t) + c_2\underset{\sim}{V}(\underset{\sim}{r},t-\Delta t) + (1-c_1-c_2)\underset{\sim}{V}(\underset{\sim}{r},t-2\Delta t), \tag{3.19}$$

with $(c_1,c_2) = (1,0)$, $(\frac{3}{2}, \frac{-1}{2})$ and $(\frac{15}{8}, \frac{-10}{8})$ respectively.

3.d Spectral solution

We first recast Eqs. (3.12) and (3.13) in a form more suitable for solution by the spectral method. We introduce a reference geopotential ϕ^* and define ϕ' as the departure of ϕ from ϕ^*. Operating on (3.12) with $\underset{\sim}{r}^+\cdot(\underset{\sim}{\nabla}x)$ and $\underset{\sim}{\nabla}\cdot$ successively, multiplying both sides of (3.13) by ϕ^* and transferring the non-linear terms to the right-hand side, we finally obtain

$$\zeta + \alpha\sin\theta D + \alpha\frac{V}{a} = L, \tag{3.20}$$

$$D - \alpha\sin\theta\zeta + \alpha\frac{U}{a} + \beta\nabla^2\phi' = M, \tag{3.21}$$

$$\phi' + \gamma D = Q, \tag{3.22}$$

where

$$\alpha = \Omega\Delta t,\ \beta = \frac{\Delta t}{2},\ \gamma = \phi^*\frac{\Delta t}{2}, \tag{3.23}$$

and

$$L = \underset{\sim}{r}^+\cdot(\underset{\sim}{\nabla}x\underset{\sim}{R}), \tag{3.24}$$

$$M = \underset{\sim}{\nabla}\cdot\ \underset{\sim}{R}\ , \tag{3.25}$$

$$Q = \left[\phi' - \phi^*\ln\left(1+\frac{\phi'}{\phi^*}\right)\right] + \left[\phi^*\ln\left(1+\frac{\phi'}{\phi^*}\right) - \gamma D\right]^-. \tag{3.26}$$

Eqs. (3.20)-(3.26) differ in two aspects from the usual spectral problem. Firstly the presence of the Coriolis terms (α) on the left-hand side of (3.20) and (3.21) and secondly the non-linear dependance of the right-hand side of (3.22) on the solution ϕ' (first square-bracketed term).

The first point is taken care of by a generalisation of the Helmholtz solver to include the Coriolis terms. This is out-lined in the appendix of Côté and Staniforth (1988), and is equivalent to a spectral model that uses truncated Hough functions as in Kasahara (1977).

The second point is handled by iteratively solving (3.20)-(3.22) for ϕ' with an appropriate initial guess for Q. We use

$$Q_{\text{initial guess}} = (\phi' - \gamma D)^- - \Delta t(\phi' D)^\circ, \tag{3.27}$$

the usual semi-implicit expression but with ϕ'° and D° obtained via time extrapolation of mesh values of ϕ' and $\underset{\sim}{V}$ [c.f. (3.19)] followed by interpolation to the midpoint ($\underset{\sim}{r}^\circ$) of the trajectory.

(a)

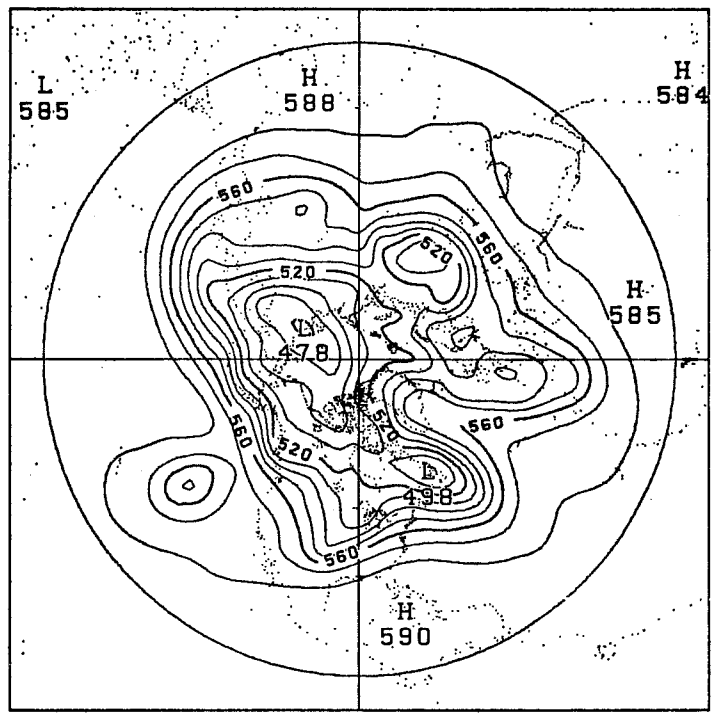

(b)

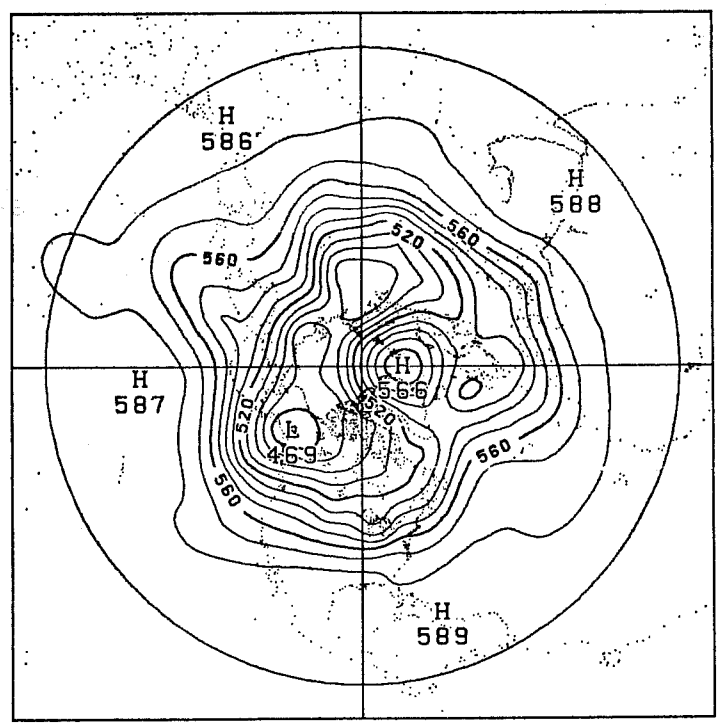

Fig. 4 Initial and forecast geopotential height fields at 120 hours (contour interval 10 dam).
(a) Initial;
(b) High-resolution (T213) Eulerian control at 120 hours;
(c) 3-time-level (T126) semi-Lagrangian at 120 hours (Δt=1 hour);
(d) 2-time-level (T126) semi-Lagrangian at 120 hours (Δt=2 hours).

(c)

(d)

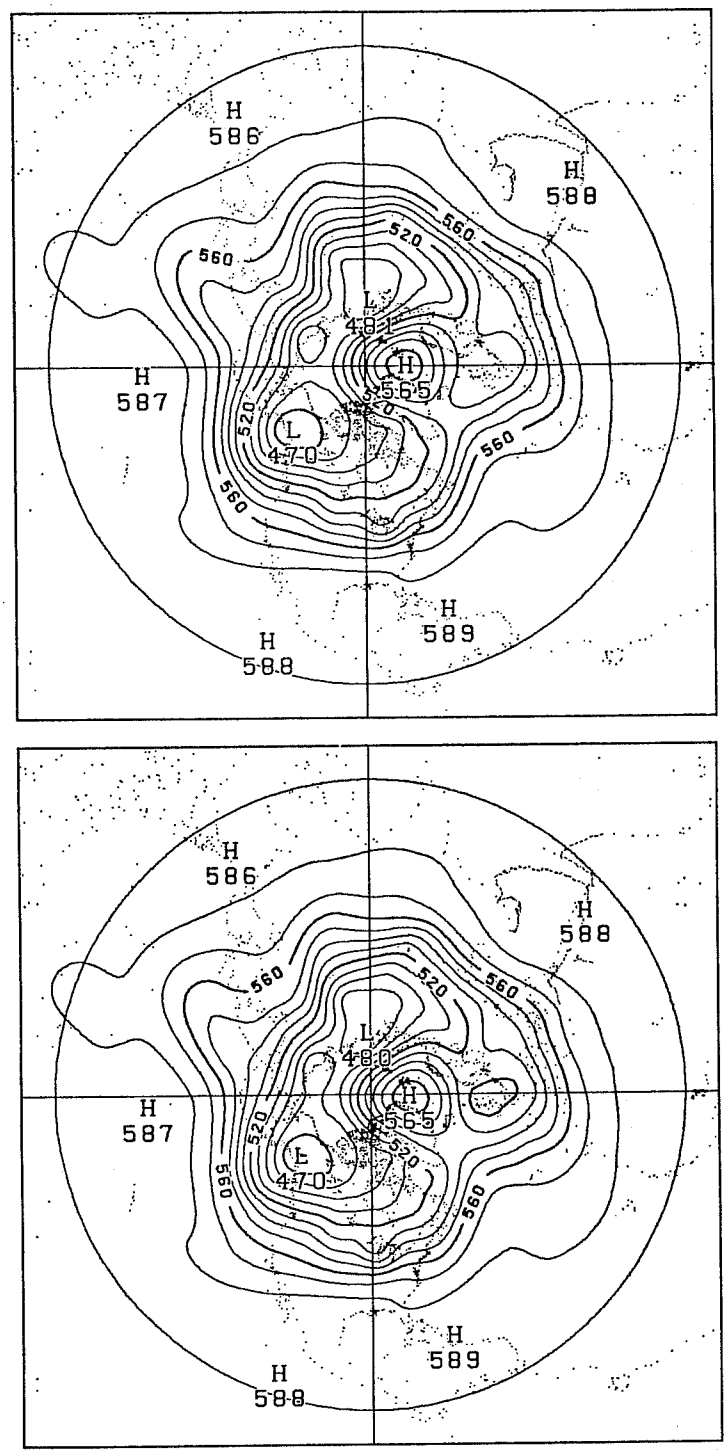

Fig. 4 Initial and forecast geopotential height fields at 120 hours (contour interval 10 dam).
(a) Initial;
(b) High-resolution (T213) Eulerian control at 120 hours;
(c) 3-time-level (T126) semi-Lagrangian at 120 hours (Δt=1 hour);
(d) 2-time-level (T126) semi-Lagrangian at 120 hours (Δt=2 hours).

The rest of the spectral discretisation is identical to that described in the companion paper. It is a triangularly truncated global spectral model with a computational Gaussian grid large enough to prevent quadratic aliasing. The required interpolation at the upstream points is bi-cubic as in Ritchie (1988).

3.e Results

To assess the accuracy and efficiency of the two-time-level semi-Lagrangian spectral model with respect to the usual three-time-level model, we performed 5-day global integrations of the two models at a resolution of T126 starting from the same data. These integrations were then verified against a T213 Eulerian integration performed with a timestep of 6 minutes.

The initial geopotential height and the resulting high-resolution Eulerian control forecast over the northern hemisphere are shown in Figs. 4a and 4b respectively. Fig. 4c displays the three-time-level forecast performed with a timestep of 1 hour while Fig. 4d displays the two-time-level forecast performed with a timestep of 2 hours. Qualitatively one sees a great similarity between the two semi-Lagrangian forecasts although one was made with a timestep twice as large. The two main features on the Eulerian map are a 469 dam low over the Yukon and a 566 dam high over the Greenland Sea which are forecast at 470 and 565 dam respectively by both semi-Lagrangian models. Among the differences we note that the 490 dam contour over the Arctic Sea in the two-time-level forecast looks more like that of the control run. The 520 dam contour west of Ireland is missing from the three-time-level forecast while it encompasses most of the United Kingdom in the two-time-level forecast.

The two models have different dispersion properties as can be judged by the trough near the Great Lakes in the control run. The three-time-level model puts this feature a little ahead while there is a slight lag in the two-time-level forecast.

For a more quantitative evaluation of the two forecasts we display in Fig. 5 the evolution of the global r.m.s. height differences between the semi-Lagrangian runs and the control run. We see that the scores are very close indeed with a small advantage for the three-time-level model at the beginning of the integration, but the curves cross and the two-time-level model has a better score near day 4.

In order to investigate the growth of time truncation error as a function of timestep length, we ran a series of forecasts for different values of Δt using the three-time-level scheme of the companion paper and the two-time-level scheme of this section. The results at 5 days are displayed in Fig. 6 where again (c.f. Fig. 3) $\Delta\tau$ is the interval over which time derivatives are calculated. For a given value of $\Delta\tau$ the two-time-level scheme requires approximately half the work of the three-time-level one. Since from Fig.1 we see that the two-time-level scheme is at least as good as the three-time-level one for fixed $\Delta\tau$, we again conclude that the two-time-level scheme is twice as efficient as the three-time-level one for given cost.

4. CONCLUDING REMARKS

In the companion paper it was shown that semi-implicit semi-Lagrangian schemes are not restricted to finite-difference models, but can be extended to include both finite element and spectral discretisations. It was found that timesteps could be increased by a factor of 5 or more, with no loss of accuracy, when compared to the corresponding semi-implicit Eulerian shallow-water models.

In the present paper we have shown in the same context that it is possible to obtain a further doubling of efficiency by using an $O(\Delta t^2)$ accurate two-time-level scheme rather than a three-time-level one, again without loss of accuracy. The described schemes are fully implicit and timesteps may thus be chosen on the basis of accuracy rather than stability.

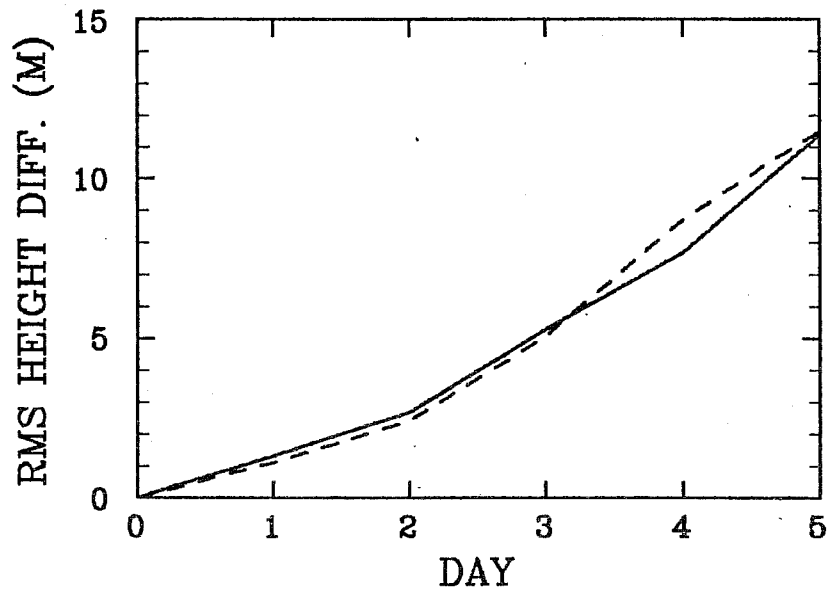

Fig. 5 Global r.m.s. geopotential height differences (m) as a function of time (days) between semi-Lagrangian runs (T126) and Eulerian control (T213).
Dotted: 3-time-level (Δt=1 hour). Full: 2-time-level (Δt=2 hours).

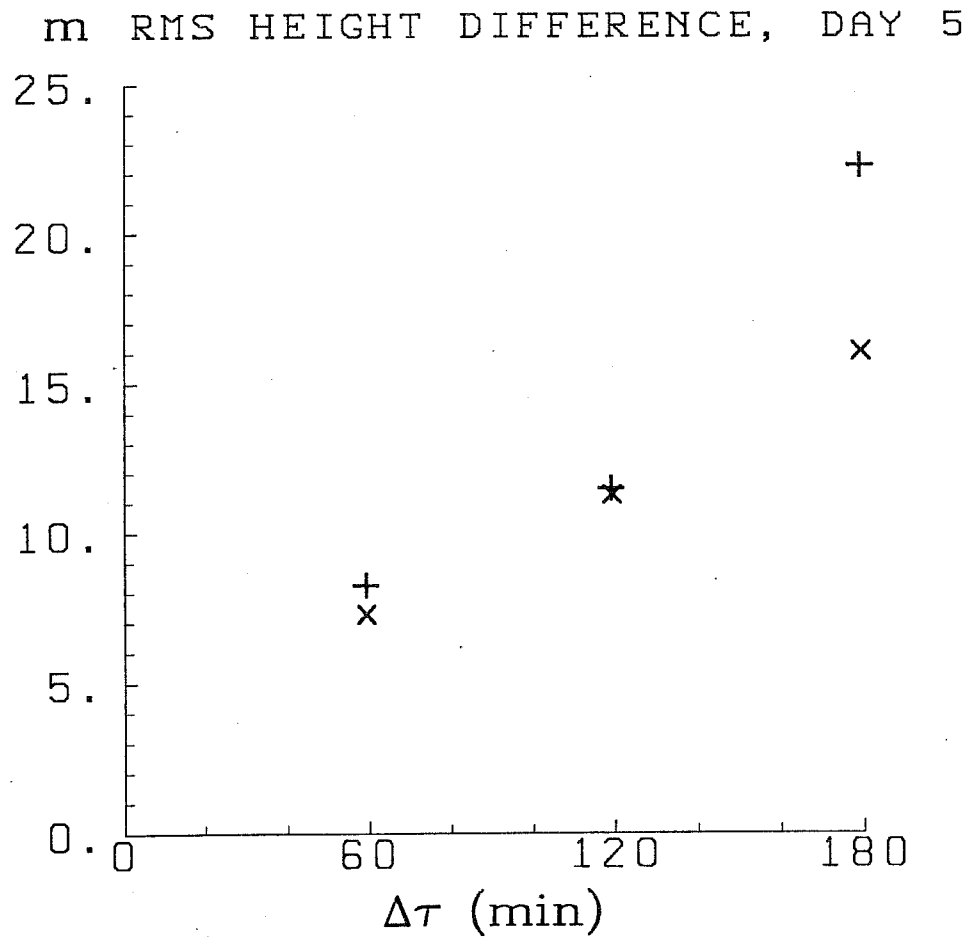

Fig. 6 Global r.m.s. differences (m) from Eulerian control, in the geopotential height field at 120 hours, as a function of Δt. "+" 3-time-level; "x" 2-time-level.

We did not address the question of whether the described two-time-level schemes may be successfully extended to the three-dimensional baroclinic equations. This is the subject of ongoing research and all we can say at present is that preliminary analyses are encouraging.

ACKNOWLEDGEMENTS

The authors gratefully acknowledge the expert typing of Diane Lespérance.

REFERENCES

Bates, J.R., and A. McDonald, 1982: Multiply-upstream, semi-Lagrangian advective schemes: Analysis and application to a multi-level primitive equation model. Mon. Wea. Rev., 110, 1831-1842.

Bates, J.R., 1984: An efficient semi-Lagrangian and alternating-direction implicit method for integrating the shallow-water equations. Mon. Wea. Rev., 112, 2033-2047.

Bates, J.R., 1988: Finite-difference semi-Lagrangian techniques for integrating the shallow-water equations on the sphere. This volume.

Côté, J., 1988: A Lagrange multiplier approach for the metric terms of semi-Lagrangian models on the sphere. Submitted to Quarterly Journal of the Royal Meteorological Society. [Preprint available from Recherche en prévision numérique]

Côté, J. and A. Staniforth, 1988: A two-time-level semi-Lagrangian semi-implicit scheme for spectral models. Submitted to Monthly Weather Review. [Preprint available from Recherche en prévision numérique].

Kasahara, A., 1977: Numerical integration of the global barotropic primitive equations with Hough harmonic expansion. J. Atmos. Sci., 34, 687-701.

McDonald, A., 1986: A semi-Lagrangian and semi-implicit two-time-level integration scheme. Mon. Wea. Rev., 114, 824-830.

McDonald, A., 1987: Accuracy of multiply-upstream, semi-Lagrangian advective schemes II. Mon. Wea. Rev., 115, 1446-1450.

McDonald, A., and J.R. Bates, 1987: Improving the estimate of the departure point position in a two-time-level semi-Lagrangian and semi-implicit model. Mon. Wea. Rev., 115, 737-739.

Pudykiewicz, J., R. Benoit and A. Staniforth, 1985: Preliminary results from a partial LRTAP model based on an existing meteorological forecast model. Atmos. Ocean, 23, 267-303.

Purser, R.J., and L.M. Leslie, 1987: A semi- implicit semi-Lagrangian finite difference scheme using high-order spatial differencing on a non-staggered grid. Submitted to Monthly Weather Review. [Preprint available from CIMSS, University of Madison, Madison, Wisconsin 53706]

Ritchie, H., 1985: Application of a semi-Lagrangian integration scheme to the moisture equation in a regional forecast model. Mon. Wea. Rev., 113, 424-435.

Ritchie, H., 1986: Eliminating the interpolation associated with the semi-Lagrangian scheme. Mon. Wea. Rev., 114, 135-146.

Ritchie, H., 1987: Semi-Lagrangian advection on a Gaussian grid. Mon. Wea. Rev., 115, 608-619.

Ritchie, H., 1988: Application of the semi- Lagrangian method to a spectral model of the shallow-water equations. Submitted to Monthly Weather Review. [Preprint available from Recherche en prévision numérique]

Robert, A.J., 1981: A stable numerical integration scheme for the primitive meteorological equations. Atmosphere-Ocean, 19, 35-46.

Robert, A.J., 1982: A semi-Lagrangian and semi-implicit numerical integration scheme for the primitive meteorological equations. J. Meteorol. Soc. (Jpn.), 60, 319-325.

Robert, A.J., T.L. Yee and H. Ritchie, 1985: A semi-Lagrangian and semi-implicit numerical integration scheme for multi-level atmospheric models. Mon. Wea. Rev., 113, 388-394.

Staniforth, A., and H. Mitchell, 1977: A semi-implicit finite-element barotropic model. Mon. Wea. Rev., 105, 154-169.

Staniforth, A., and H. Mitchell, 1977: A variable-resolution finite-element technique for regional forecasting with the primitive equations. Mon. Wea. Rev., 106, 439-447.

Staniforth, A.N. and J. Pudykiewicz, 1985: Reply to comments on and addenda to "Some properties and comparative performance of the semi-Lagrangian method of Robert in the solution of the advection-diffusion equation". Atmos. Ocean, 23, 195-200.

Staniforth, A., and C. Temperton, 1986: Semi-implicit semi-Lagrangian integration schemes for a barotropic finite-element regional model. Mon. Wea. Rev., 114, 2078-2090.

Temperton, C., and A. Staniforth, 1987: An efficient two-time-level semi-Lagrangian semi-implicit integration scheme. Q. J. Roy. Meteor. Soc., 113, 1025-1039.

Temperton, C., and H. Ritchie, 1988: Three-time-level semi-Lagrangian schemes in finite-element and spectral models. This volume.